Structure and Function of the Xenobiotic Substrate-Binding Site and Location of a Potential Non-Substrate-Binding Site in a Class π Glutathione *S*-Transferase[†,‡]

Xinhua Ji,[*,§] Maria Tordova,[||] Rosemary O'Donnell,[§] James F. Parsons,[⊥] Janet B. Hayden,[▽] Gary L. Gilliland,[||] and Piotr Zimniak[▽]

ABL-Basic Research Program, National Cancer Institute-Frederick Cancer Research and Development Center, Frederick, Maryland 21702, Center for Advanced Research in Biotechnology, University of Maryland Biotechnology Institute and National Institute of Standards and Technology, Rockville, Maryland 20850, Department of Biochemistry and Center in Molecular Toxicology, Vanderbilt University School of Medicine, Nashville, Tennessee 37232, and Departments of Medicine and of Biochemistry & Molecular Biology, University of Arkansas for Medical Sciences and VA John McClellan Memorial Hospital, Little Rock, Arkansas 72205

Received April 7, 1997; Revised Manuscript Received May 23, 1997[⊗]

ABSTRACT: Complex structures of a naturally occurring variant of human class π glutathione *S*-transferase 1-1 (hGSTP1-1) with either *S*-hexylglutathione or (9*R*,10*R*)-9-(*S*-glutathionyl)-10-hydroxy-9,10-dihydrophenanthrene [(9*R*,10*R*)-GSPhen] have been determined at resolutions of 1.8 and 1.9 Å, respectively. The crystal structures reveal that the xenobiotic substrate-binding site (H-site) is located at a position similar to that observed in class μ GST 1-1 from rat liver (rGSTM1-1). In rGSTM1-1, the H-site is a hydrophobic cavity defined by the side chains of Y6, W7, V9, L12, I111, Y115, F208, and S209. In hGSTP1-1, the cavity is approximately half hydrophobic and half hydrophilic and is defined by the side chains of Y7, F8, V10, R13, V104, Y108, N204, and G205 and five water molecules. A hydrogen bond network connects the five water molecules and the side chains of R13 and N204. V104 is positioned such that the introduction of a methyl group (the result of the V104I mutation) disturbs the H-site water structure and alters the substrate-binding properties of the isozyme. The hydroxyl group of Y7 forms a hydrogen bond (3.2 Å) with the sulfur atom of the product. There is a short hydrogen bond (2.5 Å) between Y108 (OH) and (9*R*,10*R*)-GSPhen (O5), indicating the hydroxyl group of Y108 as an electrophilic participant in the addition of glutathione to epoxides. An *N*-(2-hydroxethyl)piperazine-*N*′-2-ethanesulfonic acid (HEPES) molecule is found in the cavity between β2 and αI. The location and properties of this HEPES-binding site fit a possible non-substrate-binding site that is involved in noncompetitive inhibition of the enzyme.

Glutathione *S*-transferases (GSTs, EC 2.5.1.18)[1] catalyze the addition of the tripeptide glutathione (GSH) to xenobiotic substrates that have electrophilic functional groups. The catalytic diversity of this family of detoxification enzymes arises, in part, from the existence of at least seven distinct gene classes: α, μ, π, σ, θ, κ, and microsomal GSTs. Although each isozyme generally exhibits a relatively broad substrate selectivity, most have unique catalytic attributes that are important in defining the ability of the isozyme to metabolize a particular set of endogenous and xenobiotic electrophiles (*1*−*3*). The extent of the information concerning the precise enzyme−substrate interactions responsible for the catalytic properties has been greatly increased by the recent determinations of many three-dimensional structures of GST isozymes.

The three-dimensional structures determined by X-ray crystallographic analysis include cytosolic GSTs of class α [hGSTA1-1 from human liver (*4*)], μ [rGSTM1-1 from rat liver (*5*); hGSTM2-2 from human muscle (*6*)], π [pGSTP1-1 from pig lung (*7*); hGSTP1-1 from human placenta (*8*)], σ [sGSTS1-1 from squid digestive gland (*9*)], and θ [from *Lucillia cuprina* (*10*); from *Arabidopsis thaliana* (*11*)] and a GST from *Schistosoma japonicum* [SjGST (*12*)]. The

[†] This work was supported by NIH Grants ES07804 to Piotr Zimniak, University of Arkansas (P.Z. and J.B.H.), and R01 GM30910 to Richard N. Armstrong, Vanderbilt University (J.F.P.), and by the National Cancer Institute, DHHS, under contract with ABL (X.J. and R.O.).

[‡] The contents of this publication do not necessarily reflect the views or policies of the Department of Health and Human Services (DHHS) or the National Institute of Standards and Technology (NIST), nor does mention of trade names, commercial products, or organizations imply endorsement by DHHS, NIST, or the United States Government.

* Address correspondence to this author. Phone: (301) 846-5035. Fax: (301) 846-7101.

[§] National Cancer Institute-Frederick Cancer Research and Development Center.

[||] University of Maryland Biotechnology Institute and National Institute of Standards and Technology.

[⊥] Vanderbilt University School of Medicine.

[▽] University of Arkansas for Medical Sciences and VA John McClellan Memorial Hospital.

[⊗] Abstract published in *Advance ACS Abstracts,* July 15, 1997.

[1] Abbreviations: GSH, glutathione; GST, glutathione *S*-transferase; hGSTP1-1, class π glutathione *S*-transferase 1-1 from human placenta; rGSTM1-1, class μ glutathione *S*-transferase 1-1 from rat liver; hGSTA1-1, class α glutathione *S*-transferase from human liver; hGSTM2-2, class μ glutathione *S*-transferase from human muscle; pGSTP1-1, class π glutathione *S*-transferase from pig lung; mGSTP1-1, class π glutathione *S*-transferase from mouse liver; sGSTS1-1, class σ glutathione *S*-transferase from squid digestive gland; SjGST, glutathione *S*-transferase from *Schistosoma japonicum*; GSDNB, 1-(*S*-glutathionyl)-2,4-dinitrobenzene; CDNB, 1-chloro-2,4-dinitrobenzene; PhenO, phenanthrene 9,10-oxide; BPDE, 7,8-dihydroxy-9,10-oxy-7,8,9,10-tetrahydrobenzo[*a*]pyrene; GSHex, *S*-hexylglutathione; GSPhen, 9-(*S*-glutathionyl)-10-hydroxy-9,10-dihydrophenanthrene; GSSAc, glutathione sulfonic acid; GSpNB, *S*-(*p*-nitrobenzyl)glutathione; G-site, glutathione-binding site; H-site, xenobiotic substrate-binding site; HEPES, *N*-(2-hydroxethyl)piperazine-*N*′-2-ethanesulfonic acid; rms, root mean square.

S0006-2960(97)00805-2 CCC: $14.00

projection structure of microsomal GST has been elucidated with the use of electron crystallography at 4.0 Å resolution (*13*). Both the GSH-binding site (G-site) and the xenobiotic substrate-binding site (H-site) can be seen in these crystal structures. Three different GSH-binding modes have been observed. Class μ GSTs and SjGST share a common GSH-binding mode with the cysteinyl carbonyl hydrogen bonded to the indolyl nitrogen of W7 (*5*, *12*). In class α, π, and σ GSTs, however, the residue corresponding to W7 is F8, and the cysteinyl carbonyl points away from F8, forming a hydrogen bond with a backbone amide group (*4*, *7*, *9*). A third binding mode of GSH is represented by class θ GSTs. An invariant tyrosine residue in class α, μ, π, σ, and Sj GSTs forms a hydrogen bond with the cysteinyl sulfur. A conserved aspartic acid residue across the dimer interface is involved in GSH recognition (*4*, *5*, *7*, *9*, *12*). In class θ GSTs, however, the invariant tyrosine residue does not interact with the sulfhydryl group of GSH. Its role appears to be replaced by either a nearby serine or another tyrosine residue located in the C-terminal domain of the enzyme. Moreover, the neighboring subunit makes no contribution to GSH binding (*10*, *11*). The GSH-binding site is very well-defined for these classes of cytosolic GSTs for which three-dimensional structures are available. In contrast, only a general description of the H-site is available, primarily because for most GST isozymes there are no H-site-defining product complex structures. The H-site of rGSTM1-1 has been precisely defined in crystal structures of the enzyme in complexes with various products, including 1-(*S*-glutathionyl)-2,4,6-trinitrocyclohexadienate and 1-(*S*-glutathionyl)-2,4-dinitrobenzene (*14*), (9*R*,10*R*)- and (9*S*,10*S*)-9-(*S*-glutathionyl)-10-hydroxy-9,10-dihydrophenanthrene [GSPhen (*15*)], and *S*-(iodobenzyl)glutathione.[2] The H-site of rGSTM1-1 is a hydrophobic cavity defined by residues Y6, W7, V9, L12, I111, Y115, F208, and S209 (*15*). The three-dimensional structures can be used to explain the dramatically different stereoselectivities of the class μ isozymes (*16*). In addition to the catalytic residue Y6, a second tyrosine residue, Y115, may participate in catalysis. There is a direct hydrogen bond between the hydroxyl group of Y115 and atom O5 of (9*S*,10*S*)-GSPhen (*15*). Measurements of the offsets of site-directed mutants on the enzyme's catalytic properties also support the idea that Y115 participates in both the chemical and physical steps in catalysis (*17*).

Residue F106 in sGSTS1-1 corresponds to Y115 in rGSTM1-1. The importance of F106 has been demonstrated by kinetic characterization of the native enzyme and its site-directed mutant F106Y (*9*). The differences between the wild type and F106Y are consistent with those observed for rGSTM1-1 when the mutant Y115F was compared with the wild-type protein (*9*). These findings fully support the role of residue 115 in GST catalysis. The topologically equivalent residue in hGSTP1-1 is Y108. Recently, Parker and co-workers reported an indirect interaction between Y108 and the GSH ethacrynic acid adduct in their complex structure (*18*). A water molecule that forms a hydrogen bond (2.56 Å) with the ketone oxygen of ethacrynic acid is 3.52 Å away from the phenolic oxygen of Y108. However, there is no direct interaction between Y108 and any xenobiotic substrate or product molecule ever reported to date. Phenanthrene 9,10-oxide (PhenO) is a common xenobiotic substrate

Scheme 1

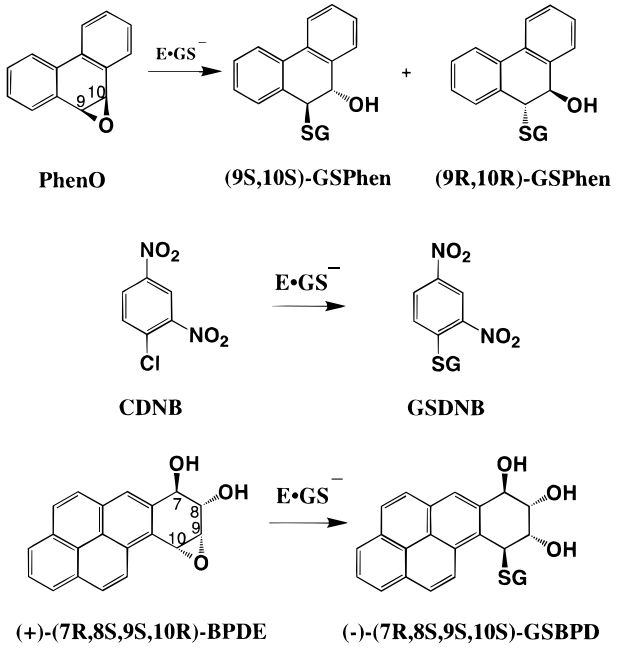

for both μ and π GSTs. The structures of rGSTM1-1 in complex with (9*R*,10*R*)- and (9*S*,10*S*)-GSPhen, the product of GSH addition to PhenO (Scheme 1), revealed the details of the architecture of the H-site in class μ GSTs. The three-dimensional structure of a class π GST in complex with the same ligands, reported in the present paper, provides the complementary information on the architecture of the H-site of class π GSTs.

Of the cytosolic GSTs, hGSTP1-1 is especially important in cancer diagnosis and therapy, because it is expressed at a high frequency and at high levels in tumors (*19*−*24*). Elevated levels of total GST and overexpression of hGSTP1-1 accompany the development of drug resistance in tumors of patients undergoing cancer chemotherapy (*25*). Using inhibitors that are selective for class π GST might be a method of overcoming drug resistance in tumor cells while sparing normal cells. However, none of the enzyme inhibitors of GST has a strong isozyme specificity (*25*), which is primarily due to a lack of information about the GSTP1-1 H-site. As a further complication, there are at least two variants of hGSTP1-1 that differ by a single methyl group (*26*, *27*). The variants, hGSTP1-1[V104] and hGSTP1-1[I104], have significantly different specific activities and affinities for xenobiotic substrates (*28*). Removing a single methyl group from the active site of rGSTA1-1 has been reported to cause a marked increase in activity (*29*). It is possible that residue 104 of hGSTP1-1 is part of the active site (*28*); however, the relevant structural evidence is not available. In an effort to elucidate the role(s) played by the residues at positions 104 and 108 in hGSTP1-1, we cocrystallized the V104 variant of hGSTP1-1 with either *S*-hexylglutathione (GSHex) or (9*R*,10*R*)-GSPhen and solved the structures of the complexes at 1.8 and 1.9 Å resolution, respectively. The H-site in hGSTP1-1 is approximately half hydrophobic and half hydrophilic, and the hydrophilic portion appears to be regulated by a hydrophobic residue at position 104. In the structure of the hGSTP1-1[V104]·(9*R*,10*R*)-GSPhen complex (Scheme 1), a direct hydrogen bond (2.5 Å) is evident between the hydroxyl group of Y108 and that

[2] X. Ji, R. N. Armstrong, and G. L. Gilliland, unpublished data.

Table 1: Summary of Data Collection for the Complexes of hGSTP1-1[V104] with GSHex and with (9*R*,10*R*)-GSPhen

	GSHex	(9*R*,10*R*)- GSPhen
X-ray source (rotating anode)	Enraf Nonius FR 591	Rigaku RU 200
detector (image plate system)	MacScience DIP 2020	MSC R-AXIS II
D_{min} (Å)	1.80	1.90
redundancy	4.23	3.92
overall completeness (%)	96.0	95.5
overall $I/\sigma(I)$	13.92	12.31
last shell completeness (%)	86.9	77.3
last shell $I/\sigma(I)$	1.81	1.92
$R_{scaling}$[a]	0.057	0.059

[a] $R_{scaling} = \sum|I-\langle I\rangle|/\sum I$. Friedel pairs were merged.

of the product, suggesting that the hydroxyl group of Y108 is an electrophilic participant in the addition of GSH to epoxides. An *N*-(2-hydroxethyl)piperazine-*N*′-2-ethanesulfonic acid (HEPES) molecule is found in the cavity between β2 and αI. The binding mode of this HEPES molecule is different from that of two previously reported HEPES molecules (*30*, *31*). The binding site of this HEPES molecule is different from other non-substrate-binding sites found in the subunit−subunit interface of SjGST (*32*) and sGSTS1-1 (*33*). The location and properties of this HEPES-binding site fit a possible non-substrate-binding site that is involved in noncompetitive inhibition of the enzyme.

EXPERIMENTAL PROCEDURES

Sample Preparation. The hGSTP1-1[V104] variant was expressed and purified as described previously (*28*). Briefly, position 313 (relative to the start codon) in the cDNA coding for hGSTP1-1[I104] was mutated (A to G) to replace Ile codon Val. The mutated cDNA was subcloned into the bacterial expression vector pET9a (Novagen), and the hGSTP1-1[V104] protein was expressed in *Escherichia coli* BL21(DE3)pLysS cells and purified to homogeneity by GSH-affinity chromatography (*34*). GSHex was purchased from Sigma. (9*R*,10*R*)-GSPhen was synthesized and purified as previously described (*35*).

Crystallization and X-ray Diffraction Data Collection. Crystals of the hGSTP1-1[V104]·GSHex complex were grown in hanging drops that initially consisted of 5.9 mg/mL protein in 0.1 M HEPES buffer (pH 6.5) containing 8.3 mM GSHex and 1.0 M buffered (pH 6.5) ammonium sulfate. The drops were equilibrated at room temperature against well solutions containing 1.9−2.0 M ammonium sulfate in 0.1 M HEPES buffer (pH 6.5). Crystals of the hGSTP1-1[V104]·(9*R*,10*R*)-GSPhen complex were obtained in an identical manner except that the pH was 7.0. Both complexes were crystallized in the *C*2 space group with the following unit cell parameters: $a = 79.4$ Å, $b = 90.8$ Å, $c = 69.2$ Å, $\alpha = \gamma = 90.0°$, and $\beta = 98.1°$. X-ray diffraction data were collected from single crystals using either a MacScience DIP2020 image plate system with an Enraf Nonius FR 501 rotating anode (45 kV per 110 mA) or an MSC R-AXIS II image plate system with a Rigaku rotating anode (50 kV per 100 mA) X-ray source. The raw data images were processed on a Silicon Graphics Indigo2 computer with a Solid Impact graphics system using the DENZO suite of programs (*36*). Each of the data sets was subsequently scaled using SCALEPACK (*36*). Data collection statistics are summarized in Table 1.

Crystal Structure Determination. The crystal structure of the hGSTP1-1[V104]·GSHex complex was solved by the molecular replacement technique (*37*) using the program AmoRe (*38*) embedded in the program suite CCP4 (*39*). The search model was the 2.8 Å dimeric structure of the hGSTP1-1[I104]·GSHex complex (*8*) with the hexyl groups of GSHex molecules and water molecules removed. Diffraction data from 4 to 10 Å resolution were included for both the rotational and translational searches. The solution was obtained with a correlation coefficient of 0.60 and a crystallographic *R*-factor of 0.39, which were improved by rigid body refinement to 0.72 and 0.33, respectively.

Crystallographic Refinement. The molecular replacement solution was first refined by using the X-PLOR (*40*) package, which reduced the crystallographic *R*-factor to 0.19 for X-ray diffraction data between 6.0 and 1.8 Å when $I/\sigma(I) \geq 1$. I104 was replaced by V104 according to the indication of difference Fourier maps contoured at 3σ and -3σ. The initiator methionine for subunit A (which is involved in intermolecular interaction) was built into the $F_o - F_c$ map contoured at 3σ without any ambiguity. Further refinement was carried out with the program suite GPRLSA (*41*) using the restrained least-squares refinement procedure of Hendrickson and Konnert (*42*, *43*) and Hendrickson (*44*, *45*). The crystallographic *R*-factor for the final model of the hGSTP1-1[V104]·GSHex complex was 0.18, which, after removing the inhibitor and water molecules, was used as the starting model for the refinement of the hGSTP1-1[V104]·(9*R*,10*R*)-GSPhen complex. (9*R*,10*R*)-GSPhen was clearly seen in the $F_o - F_c$ map. The final *R*-factor was also 0.18 for X-ray diffraction data between 6.0 and 1.9 Å when $I/\sigma(I) \geq 1.5$. The O program suite (*46*) was used on an Indigo2 computer with a Solid Impact graphics system for model building and adjustments.

The entire model was checked and adjusted after each cycle of refinement. Complete models of the GSH conjugates were built into the difference Fourier map contoured at 2σ. Water molecules were located in the difference Fourier maps as peaks higher than 3σ. After all the identifiable water molecules were found, they were verified by a series of omit maps (*47*) with a set of 100 molecules deleted each time. This procedure was performed in ascending order starting from the bottom of the list of water molecules ranked according to the parameter OCC^2/B (*48*), the ratio of the square of the fractional occupancy factor (OCC) of the oxygen atom position and the crystallographic temperature factor (*B*). All X-ray diffraction data were included in electron density map calculations. A summary of the crystallographic refinement is found in Table 2. The structure factors and final coordinates for both structures have been deposited in the Brookhaven Protein Data Bank (*49*) under the identification codes 1PGT for the hGSTP1-1[V104]·GSHex complex and 2PGT for the hGSTP1-1[V104]· (9*R*,10*R*)-GSPhen complex.

RESULTS

Overall Structures. Figure 1 schematically illustrates the structure of subunit A of the hGSTP1-1[V104]· (9*R*,10*R*)-GSPhen complex. The structure of the hGSTP1-1[V104]·GSHex complex shares every detail with this structure except that GSHex does not interact directly with Y108. The final model of the hGSTP1-1[V104]·GSHex complex includes 419

Table 2: Summary of the Least-Squares Refinement Statistics for the Complexes of hGSTP1-1[V104] with GSHex and with (9*R*,10*R*)-GSPhen

	GSHex	(9*R*,10*R*)-GSPhen
resolution range (Å)[a]	6.0−1.8	6.0−1.9
reflections used with $I \geq$	1σ(*I*)	1.5σ(*I*)
number of reflections used	38 244	30 838
crystallographic *R*-factor[b]	0.182	0.183
number of amino acid residues	419[c]	419[c]
ligands	2 GSHex and 2 HEPES	2 GSPhen, 2 HEPES, and 1 $(SO_4)^{2-}$
number of water molecules	329	344
rms deviations from ideal distances (Å)		
bond distances	0.015	0.017
bond angles	0.033	0.034
planar 1−4 distances	0.071	0.072
rms deviations from ideal chirality (Å^3)	0.199	0.183
thermal parameter correlation (mean/$\Delta\beta$)		
main chain bond	0.723	0.726
main chain angle	1.165	1.225
side chain bond	1.389	1.298
side chain angle	2.034	1.995

[a] Data used for refinement. [b] The crystallographic *R*-factor $= \sum_{hkl}||F_o| - |F_c||/\sum_{hkl}|F_o|$. [c] A methionine residue was observed at the N terminus of one subunit.

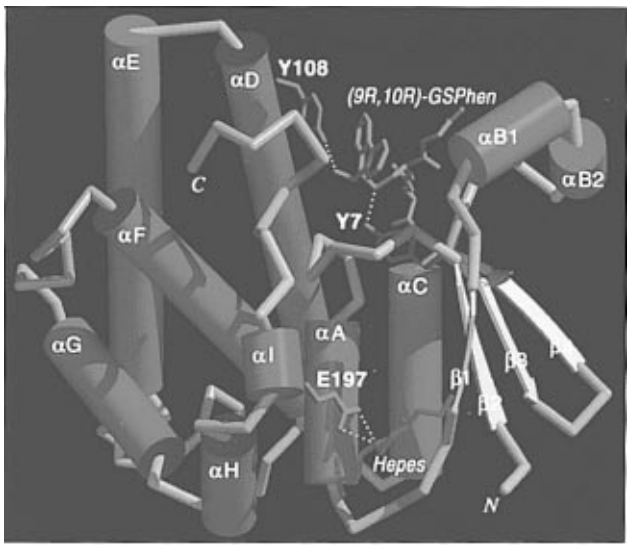

FIGURE 1: Schematic representations of one subunit of the hGSTP1-1·(9*R*,10*R*)-GSPhen complex. The α helices labeled αA−αI are represented by blue cylinders. The β strands designated β1−β4 are shown as yellow arrows. The gray pipes illustrate loop structures. The product complex (9*R*,10*R*)-GSPhen is shown as a stick model in pink and the HEPES molecule in green. The side chains of Y7, Y108, and E197 are represented as stick models in red and the hydrogen bonds as white dotted lines. The illustrations were prepared by using TkRaster3D (by Hillary Gilson, National Institute of Standards and Technology, http://indigo15.carb.nist.gov/TkRaster3D), the newest version of Raster3D (*69*) with enhanced features.

amino acid residues, 2 GSHex molecules, 2 HEPES molecules, and 329 water molecules. The final model of the hGSTP1-1[V104]·(9*R*,10*R*)-GSPhen complex includes 419 amino acid residues, 2 GSHex molecules, 2 HEPES molecules, 1 sulfate anion, and 344 water molecules (Table 2). Both structures have a crystallographic *R*-factor of 0.18 for X-ray diffraction data with resolution of higher than 6 Å and a signal/noise ratio of better than 1. Both structures have good geometry. The root mean square (rms) deviations for bond distances and angle distances are ≤0.017 and ≤0.034 Å, respectively (Table 2). More than 91% of the residues exhibit the most favorable $\phi-\psi$ relationship according to the protein structure verification procedure PROCHECK (*50*). The structures of the two hGSTP1-1[V104]·product complexes are quite similar except in the immediate vicinity of the active site. The rms deviation for all 419 α-carbon atoms between the two dimeric molecules is 0.21 Å. The fold of the polypeptide chain (Figure 1) is virtually the same as that reported by Reinemer and his colleagues [1GSS (*8*)] except that helices αB1 and αG are longer by one residue than those of 1GSS. Each subunit contains two domains, a smaller α/β domain and a larger α domain. The α/β domain consists of 80 amino acid residues that form the secondary structure elements β2, αA, β1, αB1, αB2, β3, β4, and αC. The α domain contains six α helices (αD−αI, Figure 1) and two 3_{10} helices located between αE and αF and between αF and αG. A methionine residue that can be seen at the N terminus of subunit A in both hGSTP1-1[V104] structures is not seen in subunit B. The initiator methionine in subunit A is involved in intermolecular interactions with symmetry-related molecules, causing this methionine to assume a defined conformation that is observed in the electron density map.

Subunit−Subunit Interactions. In their biologically active form, cytosolic GSTs are dimeric. Molecular recognition between the subunits is class specific. Heterodimerization occurs only within the same gene class. The two subunits contact each other primarily by interactions between domain I of one subunit and domain II of the adjacent subunit. A hydrophilic channel that runs through the dimer is coincident with either a crystallographic 2-fold axis as in class σ GST (*9*) or a noncrystallographic 2-fold axis as observed in hGSTP1-1[V104] structures (this work) and most other GST structures. The insertion of the side chain of F56 from domain I of one subunit into a pocket formed by I98, Q102, L136, Y137, and F140 from domain II of the second subunit forms a hydrophobic "lock" between the two subunits of rGSTM1-1 (*5*). This lock is also seen in other isozymes from the α and π gene classes and from *S. japonicum*, but not in sGSTS1-1 (Table 3), providing a structural clue to the evolution of GSTs. The unique dimer interface of sGSTS1-1 suggests that the class σ enzyme diverged from the ancestral precursor prior to the divergence of the precursor gene for the α, μ, and π classes (*9*). In class π GSTs, the corresponding lock residues M89, G93, P126, F127, and L130 are conserved in pig (*7*), mouse (*51*), and human [(*8*), this work] enzymes. The "key" residue is either a phenylalanine or a tyrosine, depending on the subunit

Table 3: Lock and Key Residues Involved in the Hydrophobic Interaction between the Two Subunits of GSTs from Class α, μ, and π Gene Classes and from *S. japonicum*

isozyme	key	lock				
hGSTA1-1 (*4*)	F52	M94	G98	A135	F136	V139
rGSTM1-1 (*5*)	F56	I98	Q102	L136	Y137	F140
rGSTM2-2[b]	F56	V98	Q102	L136	Y137	F140
hGSTM2-2 (*6*)	F56	I98	Q102	L136	Y137	F140
pGSTP1-1 (*7*)	F47	M89	G93	P126	F127	L130
hGSTP1-1 (*8*)	Y49	M91	G95	P128	F129	L132
mGSTP1-1 (*51*)	Y49	M91	G95	P128	F129	L132
SjGST (*12*)	F51	M93	A97	M131	F132	R135
sGSTS1-1 (*9*)	—[a]	E89	T93	F129	L130	L133

[a] The key residue is missing in the class σ isozyme. [b] X Ji, R. N. Armstrong, and G. L. Gilliland, unpublished data.

types: phenylalanine in pGSTP1-1 (*7*) and tyrosine in mGSTP1-1 (*51*) and hGSTP1-1 (*8*). According to the high-resolution structures of hGSTP1-1[V104], a hydrogen bond, ranging from 2.77 to 2.95 Å, is formed between the hydroxyl group of the key residue, Y49, and the carbonyl oxygen of one of the lock residues of the associated subunit, M91. The lock-and-key interaction is enhanced by the additional electrostatic interactions in mouse and human π GSTs.

Protein−Product Interactions. Figure 2 illustrates the omit maps for the two product molecules bound to hGSTP1-1[V104] in subunit A. The corresponding initial difference maps for the product complexes are similar to the omit maps calculated at the final stage of the refinement. The electron density maps of the product complexes in the active site of subunit B are of similar quality. Modeling of the product posed no particular problems in the refinement. No disordering of the product molecules is seen. Both product molecules are bound in essentially a single conformation. The distance between the hydroxyl group of Y7 and the thioether group of the product complexes is well-defined with a distance of 3.2 Å in both subunits for both structures. Although the rms deviation for all Cα atoms between the present structure and other reported class π GSTs is as large as 0.69 Å, interactions between the protein and the glutathionyl portion of the two products are basically identical to those observed previously (*7*, *8*, *51*).

The (9*R*,10*R*)-GSPhen molecule bound to the active site together with the H-site-defining residues of hGSTP1-1[V104] are shown in Figure 3a. The phenanthrenyl moiety can make van der Waals contacts with residues Y7, F8, and V10 from domain I and Y108 and G205 from domain II. There is a short hydrogen bond with an O−O distance of 2.5 Å between the hydroxyl group of Y108 and the 10-hydroxyl group of the product molecule, (9*R*,10*R*)-GSPhen. In addition, the 10-hydroxyl group of the product molecule forms a hydrogen bond with one of the five active site water molecules. The five water molecules, numbers 1−5, form a hydrogen bond network with R13 and N204, NE(R13)···Wat1···Wat2···Wat3···OD1(N204)···Wat4···Wat5. In addition, water 1 is involved in GSH binding. Water 2 is also hydrogen bonded to water 5. Water 3 interacts with the 10-hydroxyl group of the product. Water 4 extends the hydrogen bond network into a solvent channel that leads to the surface of the protein (see Figure 5). Water 5 forms a hydrogen bond to atom NE of R100 (not shown in Figure 3a). These five water molecules, together with R13 and N204, make up the hydrophilic portion of the H-site. A view from "behind" the H-site is shown in Figure 4a for the GSHex complex. When a xenobiotic substrate does not have a hydrophilic group, water 3 interacts with the hydroxyl group of Y108 instead of the xenobiotic molecule (Figures 3a and 4a). The hydrophilic portion of the H-site preferentially interacts with hydrophilic groups of the xenobiotic substrate whenever feasible. Furthermore, V104 occupies a position such that the introduction of the methyl group, caused by the V104I mutation, dramatically disturbs the hydrophilic portion of the H-site (Figures 3a and 4a).

As shown in Figure 5, the solvent channel has four walls, for the purpose of this description designated as front, left, back, and right. The front wall is composed of the side chains of two isoleucine residues, I161 and I203. The side chain of R11 makes up the left wall. The back wall consists of the side chains of A15 and Y198. The hydroxyl group of Y198 starts a hydrogen bond chain that forms the wall on the right side. The hydrogen bond chain involves OH(Y198), Wat650, OD1 and OD2(D157), and NH1 and NH2(R100). The well-defined solvent channel contains three water molecules, 4a, 4b, and 4c (Figure 5). Water 4a is hydrogen bonded to water 4, the carboxyl group of G12, OD2 of D157, and water 4b. In addition to the hydrogen bond to 4a, water 4b forms hydrogen bonds to OD1 of D157 and to water 4c which is hydrogen bonded to OH(Y198) and NH1(R11). The channel opens to more ordered water molecules and bulk solvent.

Solvent Structure. A total of 326 ordered water molecules are observed in the crystal structure of the hGSTP1-1[V104]·GSHex complex, of which 279 form hydrogen bond(s) to the protein. By comparison, 294 out of 344 water molecules observed in the (9*R*,10*R*)-GSPhen complex are hydrogen bonded to the enzyme. Each water molecule included in the final model of the two structures is hydrogen bonded to other atom(s). One sulfate anion is found in the (9*R*,10*R*)-GSPhen complex. The existence of this sulfate anion was confirmed by omit map calculations. It is within hydrogen bond distance (3.5 Å) of atoms NH1 and NH2 of R186 and four nearby water molecules. No sulfate is observed in the GSHex complex. One HEPES molecule is bound in the cavity between secondary structure elements β2 and αI and on top of αA and αC (Figure 1) in both subunits of both structures. The electrostatic interaction between the HEPES molecule and the protein includes direct hydrogen bonds with E197, K29, and E30 and indirect hydrogen bonds with A22 and K188 via water molecules (Figure 6a). These interactions are conserved in both subunits of both hGSTP1-1[V104] structures.

DISCUSSION

Hydrophobic Lock with Electrostatic Enhancement. Table 3 lists the hydrophobic lock and key residues for class α, μ, π, and Sj GSTs and the corresponding residues in squid GST (class σ). This structural feature, the hydrophobic lock-and-key interaction, exists in all of the known GST structures with the exception of the squid enzyme, and it has been proposed (*9*) that class σ GSTs evolutionarily diverged before class α, μ, and π and after class θ GSTs. From this point of view, SjGST (*12*) would diverge with the class α, μ, and π GSTs. It will be interesting to find out whether the hydrophobic lock exists in class θ GSTs and, consequently, to determine to what degree this structural feature is a marker for the evolution of GSTs. Although the hydrophobic lock

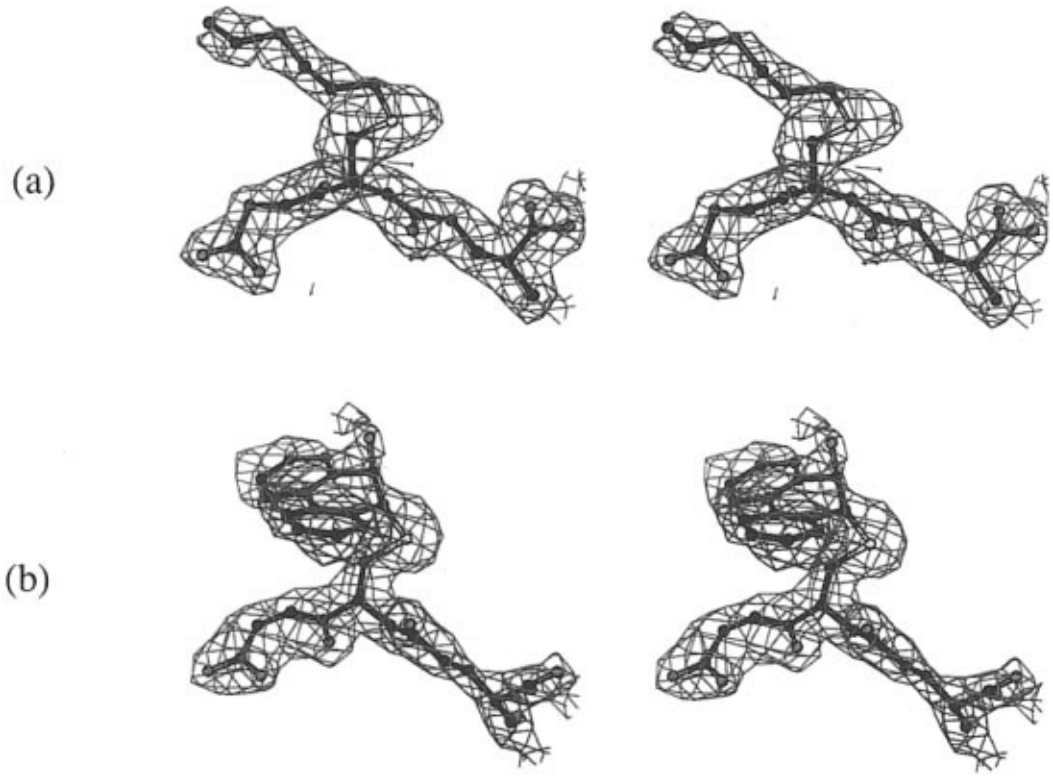

FIGURE 2: Stereoview of omit $2F_o - F_c$ maps, contoured at 1σ, of the product molecules in the complex structure of hGSTP1-1 with (a) GSHex and (b) (9*R*,10*R*)-GSPhen. The product molecules are represented by ball-and-stick models with carbon in black, oxygen in red, and nitrogen in blue. The electron density is displayed as green nets. The representation was prepared by using Bobscript (R. Esnouf, robert@s151h16.rega.kuleuven.ac.be), the extended version of Molscript (*70*).

exists in all class π structures, a new feature is seen in mouse and human π GSTs. In mGSTP1-1 and hGSTP1-1, the lock-and-key interaction is enhanced by an electrostatic interaction that can occur because the key residue is tyrosine instead of phenylalanine (Table 3). A hydrogen bond, ranging from 2.77 to 2.95 Å, is formed between the hydroxyl group of the key residue, Y49, and the carbonyl oxygen of one of the lock residues from the associated subunit, M91. Although hydrogen bonding would enhance the subunit−subunit interaction in mouse and human GSTs, the importance of such an enhancement is not clear.

GSH-Binding Site (*G-Site*). A conserved tyrosine was originally identified as a catalytic residue in the G-site on the basis of the three-dimensional protein structure (*7*). It was proposed that this residue lowers the pK_a of the GSH sulfhydryl group. The importance of Y6 in catalysis has been confirmed by site-directed mutagenesis (*52*). In rGSTM1-1, Y6 is assisted by a "nephotic" effect, a second-sphere electrostatic interaction between the OG of T13 and the π electron cloud of Y6 (*53*). For class μ GSTs, the distance between the hydroxyl group of Y6 and the sulfur atom of GSH is always 3.2 Å unless the xenobiotic moiety of the product is not bound in the H-site, i.e., for 1-(*S*-glutathionyl)-2,4-dinitrobenzene (GSDNB). GSDNB is the product of GSH and 1-chloro-2,4-dinitrobenzene (CDNB, Scheme 1), which is in a conformation when it is leaving the active site (*14*). The O−S hydrogen bond distance can also be established for class π GSTs. Table 4 summarizes this distance for seven crystal structures of class π GSTs now available. Of the 14 O−S distances, seven are 3.2 Å, one is less than 2.8 Å, and six are greater than 3.5 Å. Six out of eight O−S distances in high-resolution ($\leq$2.0 Å) structures are 3.2 Å. The distance between the sulfur atom and the phenolic oxygen calculated by using *ab initio* molecular theory (*54*) and model compounds is 3.2 Å as well. Therefore, we propose that the O−S hydrogen bond distance in enzyme·product complexes of class π GSTs is 3.2 Å. Other details of the G-site are identical to those previously established (*8*, *51*, *55*). Although the interactions between the protein and the hexyl moiety of GSHex are identical to those of available π GST structures, the interaction between the phenanthrenyl moiety of the product molecule and the enzyme reveals new features of the xenobiotic substrate-binding site in class π GSTs.

Xenobiotic Substrate-Binding Site (H-Site). The 2.5 Å hydrogen bond between the 10-hydroxyl group of the product and the hydroxyl group of Y108 is the first structural evidence directly indicating that Y108 participates in catalysis. The ring opening and hydroxylation of the epoxide are probably facilitated by the functional group of Y108 together with the H-site-bound water molecules. As summarized in the results, there are five H-site water molecules, of which water 3 interacts with the 10-hydroxyl group of the product (Figure 3a). Atom OD1 of N204 bridges water 3 and water 4, and water 4 extends the network into the solvent channel that leads to the surface of the enzyme. The five H-site water molecules are conserved in pGSTP1-1 (*55*), mGSTP1-1 (*51*), and hGSTP1-1[V104] (this work). Also conserved is the solvent channel that contains three ordered water molecules (Figure 5). All three water molecules are observed in nine out of 12 subunits in six crystal structures of class π GSTs, including the hGSTP1-1·GSHex complex (1PGT) at 1.8 Å and the hGSTP1-1·(9*R*,10*R*)-GSPhen complex (2PGT) at 1.9 Å (this work), the mGSTP1-1·GSH-sulfonic acid complex (1GLP) at 1.9 Å, the mGSTP1-1·nitrobenzyl-GSH complex (1GLQ) at 1.8 Å and the

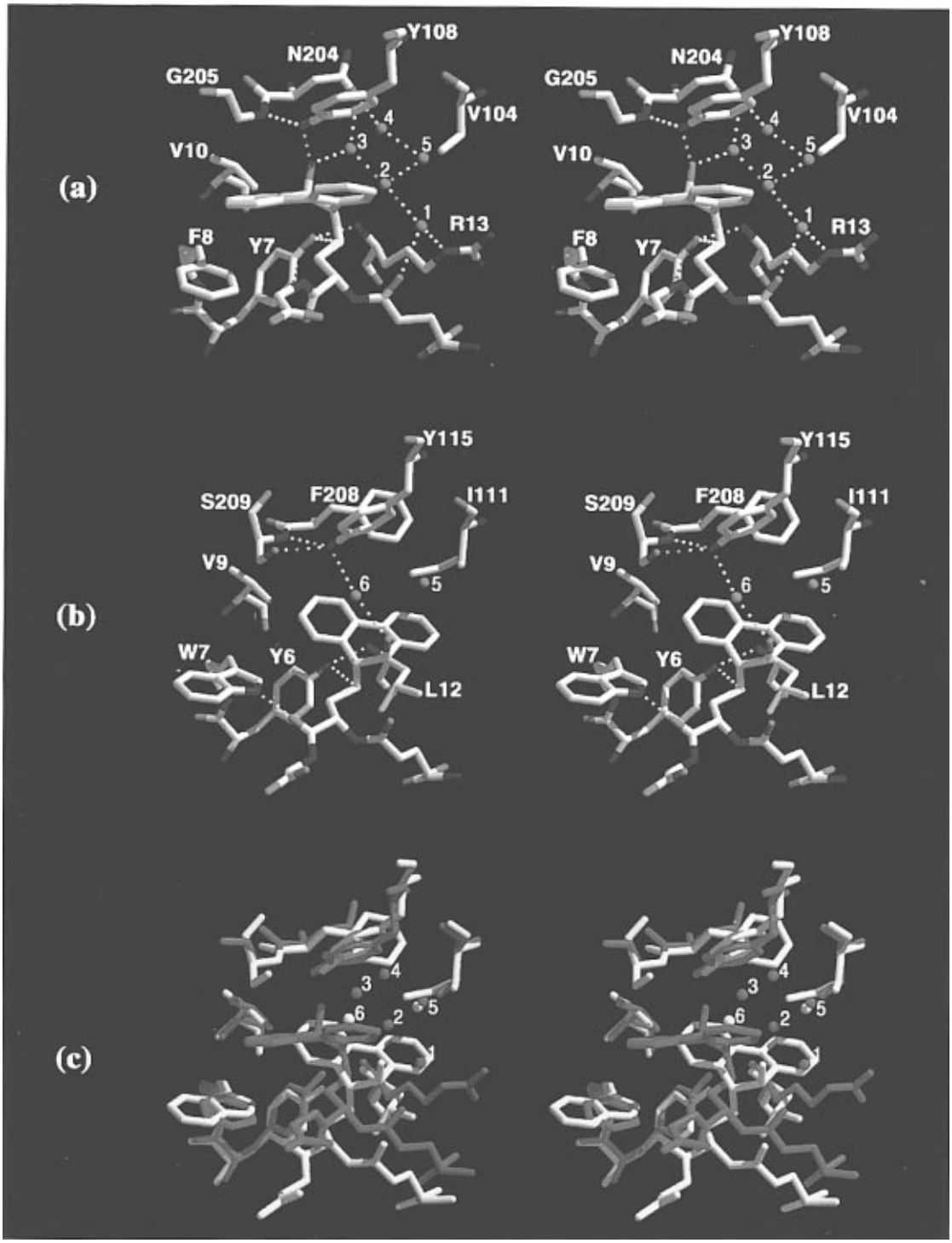

FIGURE 3: Stereoview of a ball-and-stick model of the H-site of (a) hGSTP1-1[V104] in complex with (9*R*,10*R*)-GSPhen (2PGT, this work) and (b) rGSTM1-1 in complex with (9*R*,10*R*)-GSPhen [3GST (*5*)]. The H-site-defining residues are labeled for hGSTP1-1[V104] (a) and for rGSTM1-1 (b). The CPK color scheme is shown with carbon in gray, oxygen in red, nitrogen in blue, and sulfur in yellow. H-site-bound water molecules are illustrated as balls and are labeled numerically from 1 to 6. The H-site of hGSTP1-1[V104] is compared with that of rGSTM1-1 (c). Stick models are used in cases (c) where hGSTP1-1[V104] is illustrated in blue and rGSTM1-1 in yellow. The representation was prepared by using TkRaster3D (see the legend to Figure 1 for details).

mGSTP1-1·GSHex complex (2GLR) at 2.2 Å (*51*), and the pGSTP1-1·GSH sulfonate complex (2GSR) at 2.1 Å (*55*). Water 4c is not observed in three out of the 12 subunits, whereas 4a and 4b are well-defined in all 12 subunits. This network may facilitate proton transfer during catalysis.

Unlike the H-site of class π GSTs, the H-site in class μ GSTs (Figure 3b) is a hydrophobic cavity defined by residues Y6, W7, V9, L12, I111, Y115, F208, and S209 (*15*). Two water molecules are found in the H-site of rGSTM1-1. Water 5 in rGSTM1-1 (Figure 3b) is a structural water located within the hydrogen bond distance of O(A11), NH1(R107), OE1(Q165), and NE2(Q165) and is about 5 Å away from I111. This water molecule is different from water 5 in class π GSTs (Figure 3a) which is part of the water network in the H-site, interacts mainly with other H-site water molecules, and is within 3.5 Å of V104. Water 6 in rGSTM1-1 (Figure 3b) bridges the hydroxyl group of the catalytic residue Y115 and the hydroxyl group of the

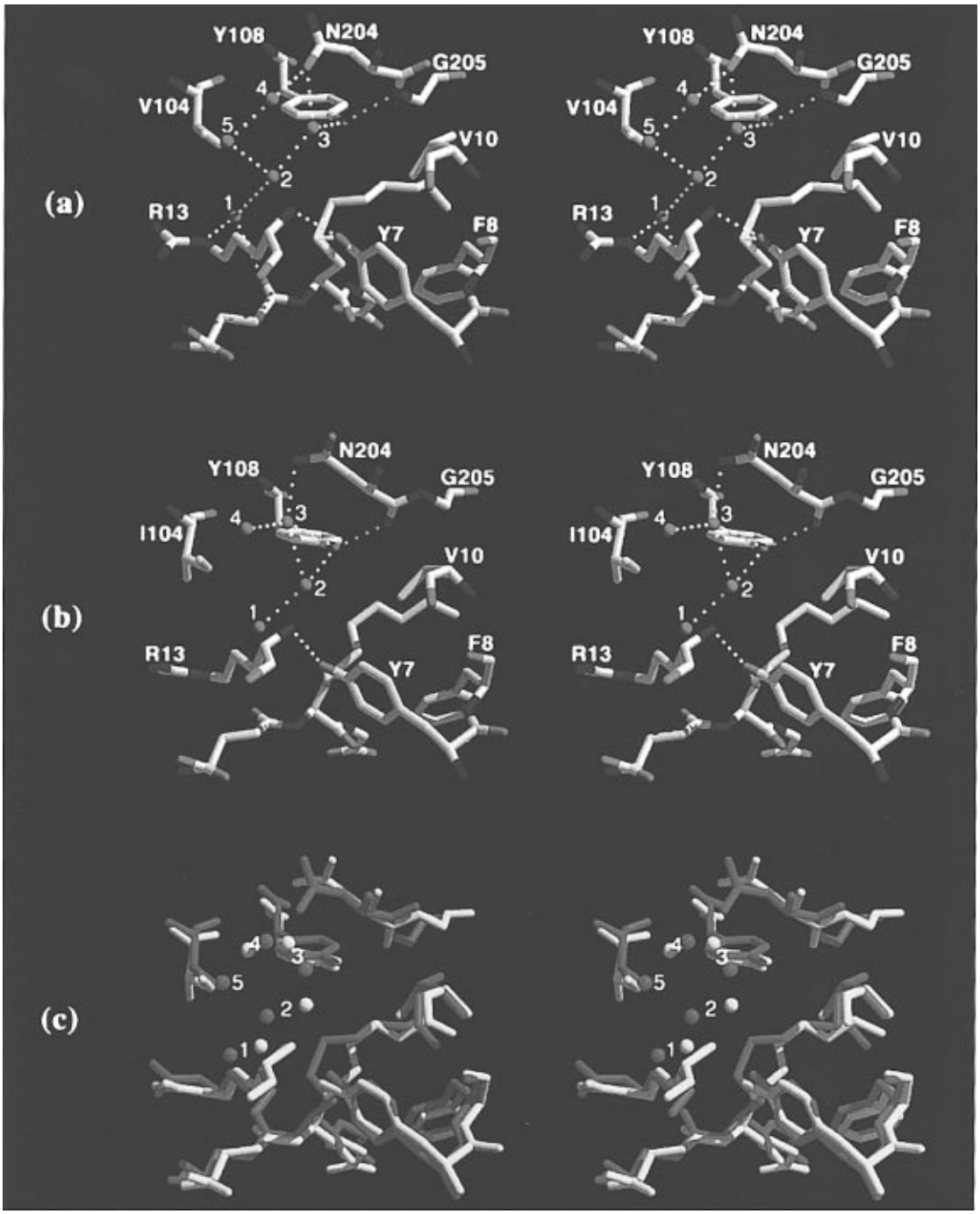

FIGURE 4: Stereoview of a ball-and-stick model of the H-site of (a) hGSTP1-1[V104]·GSHex (1GPT, this work) and (b) hGSTP1-1[I104]·GSHex [1GSS (*8*)]. The H-site-defining residues are labeled for hGSTP1-1[V104] (a) and for hGSTP1-1[I104] (b). The CPK color scheme is shown with carbon in gray, oxygen in red, nitrogen in blue, and sulfur in yellow. H-site-bound water molecules are illustrated as balls and are labeled numerically from 1 to 5. The H-site of hGSTP1-1[V104] is compared with that of hGSTP1-1[I104] (c). Stick models are used in cases (c) where hGSTP1-1[V104] is illustrated in blue and hGSTP1-1[I104] in yellow. The representation was prepared by using TkRaster3D (see the legend to Figure 1 for details). The relative orientation of this representation and Figure 3 is 180° rotation about the vertical axis.

product's phenanthrenyl moiety. The H-site residues of rGSTM1-1 correspond exactly to those of the H-site in class π GSTs. In other words, the H-site in class π GSTs occupies the same position in three-dimensional space as in class μ GSTs. The H-sites of the two proteins are compared in Figure 3c. The alignment is achieved by optimizing the superposition of the H-site-defining residues. The product (9*R*,10*R*)-GSPhen has similar but not identical interactions with the protein. First, the GSH-binding mode is different, as the result of the F8-W7 substitution. In class μ GSTs, the cysteinyl carbonyl of GSH is hydrogen bonded to the indolyl nitrogen of W7 (Figure 3b) (*5*). In class π GSTs, however, the cysteinyl carbonyl points away from F8 and forms a hydrogen bond with a backbone amide group (*4*, *7*, *9*). Second, the H-site water network in class π GSTs displaces the hydrophobic phenanthrenyl moiety from the hydrophilic portion of the H-site such that the conformation of the product (9*R*,10*R*)-GSPhen, especially the conformation around the SG2−CA4 single bond, is significantly different from that observed in rGSTM1-1. The torsion angle CB2−SG2−CA4−CB4 is 51° in hGSTP1-1[V104], whereas it is −89° in rGSTM1-1 (Figure 3c). Third, in both class π and

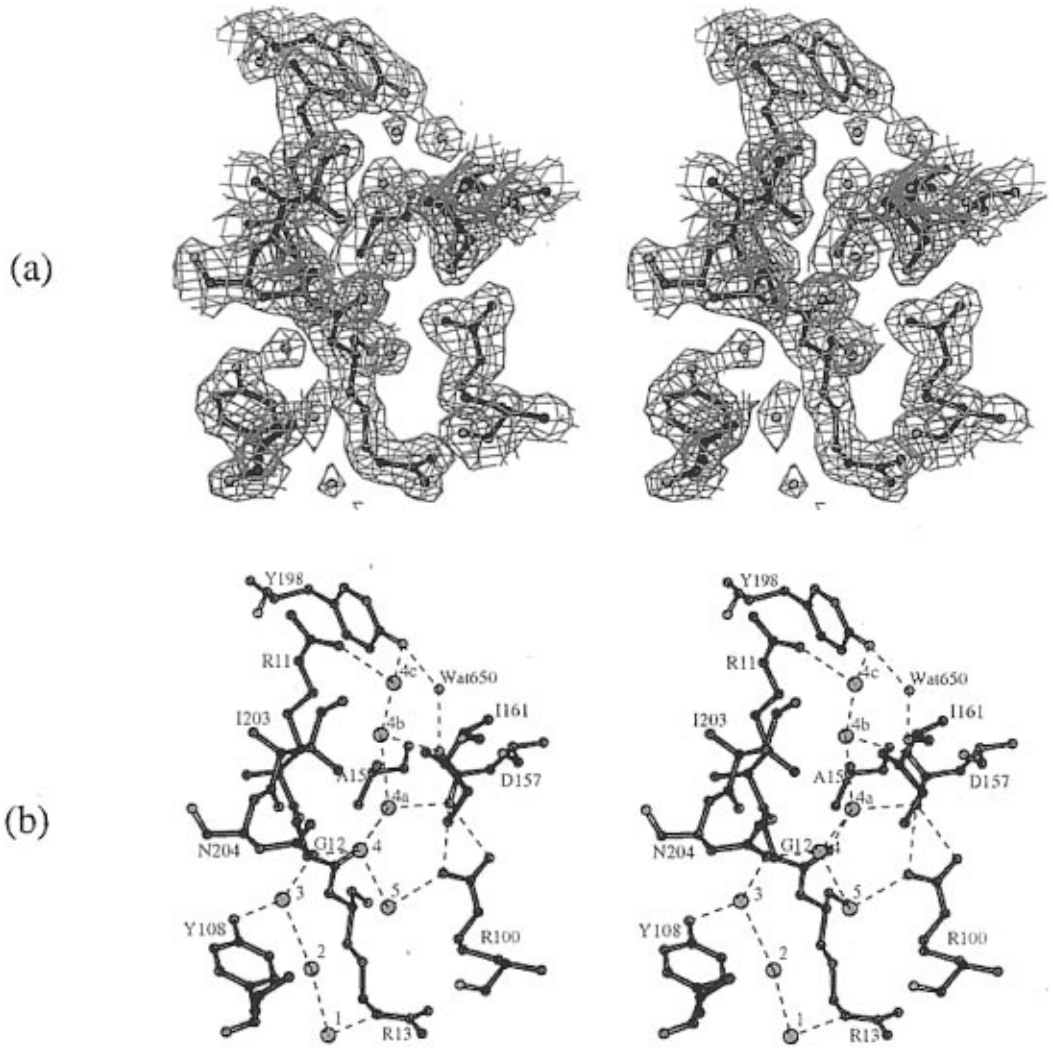

FIGURE 5: Stereoview of the solvent channel that connects the hydrophilic portion of the H-site to the surface of the protein for subunit A of hGSTP1-1[V104] in complex with GSHex at 1.8 Å resolution. The water molecules in the solvent channel are the continuation of the water network that is part of the H-site in class π GSTs. The protein is represented as a ball-and-stick model with oxygen in red and other atoms in black. Electron density, the final $2F_o - F_c$ map contoured at 1σ, is illustrated in panel a as a green net. In panel b, the H-site-bound water molecules are labeled from 1 to 5 and those in the solvent channel as 4a, 4b, and 4c, indicating that the extension of H-site-bound water network is from water 4. Eight water molecules, 1−5 and 4a−4c, are highlighted as balls larger than Wat650 which is involved in the formation of the solvent channel (see the text). Hydrogen bonds are represented by dashed lines. The representation was prepared by using Bobscript (see the legend to Figure 2 for details).

class μ GSTs, a conserved tyrosine residue from domain II interacts with the 10-hydroxyl group via its hydroxyl group. In hGSTP1-1[V104], a strong hydrogen bond with an O−O distance of less than 2.5 Å is formed between (9*R*,10*R*)-GSPhen and Y108, whereas in rGSTM1-1, this interaction involves a water molecule, although in the rGSTM1-1·(9S,10S)-GSPhen complex there is a direct hydrogen bond (*15*). The side chain of this tyrosine of rGSTM1-1 and sGSTS1-1 is appropriately positioned to provide electrophilic assistance in the addition of GSH to epoxides and to reduce the rates of product release in the reaction of GSH with CDNB (*9, 17*). For example, the ability of the Y115F mutant of rGSTM1-1 to catalyze the addition of GSH to PhenO is severely impaired because the rate-limiting step for this reaction is chemical. In contrast, the Y115F mutant is a better catalyst with CDNB, because the physical step of product dissociation is rate-limiting in this reaction (CDNB, Scheme 1). The enhanced rates of product release in the mutant can be ascribed to the loss of hydrogen bonds between the hydroxyl group of Y115 and the hydroxyl and main chain NH groups of S209, interactions that may block the channel to the active site or inhibit the segmental motion of the protein (*15, 17*). We predict that site-directed mutant Y108F of GSTP1-1 should show reduced catalytic ability toward PhenO but enhanced ability toward CDNB.

Seven out of the eight H-site-defining residues (Y7, F8, V10, R13, Y108, N204, and G205) are conserved in human, mouse, and pig GSTP1-1 proteins. The only residue that varies is that at position 104 which is occupied by alanine in pGSTP1-1 (*55*), valine in mGSTP1-1 (*51*), and either valine (this work) or isoleucine (*8*) in hGSTP1-1. As expected, an alanine residue at position 104 in pGSTP1-1 does not affect the structured water molecules in the hydrophilic portion of the H-site. However, when residue 104 is an isoleucine, the hydrophilic portion of the H-site is disturbed. The disturbance has four aspects (Figure 4b). First, water 5 is displaced by the introduction of the methyl group. Second, waters 1 and 4 move toward the position from which water 5 is displaced. Third, water 1 is no longer hydrogen bonded to atom NE of R13, and fourth, the continuation of the hydrogen bond network to the water molecules in the solvent channel is interrupted. Although

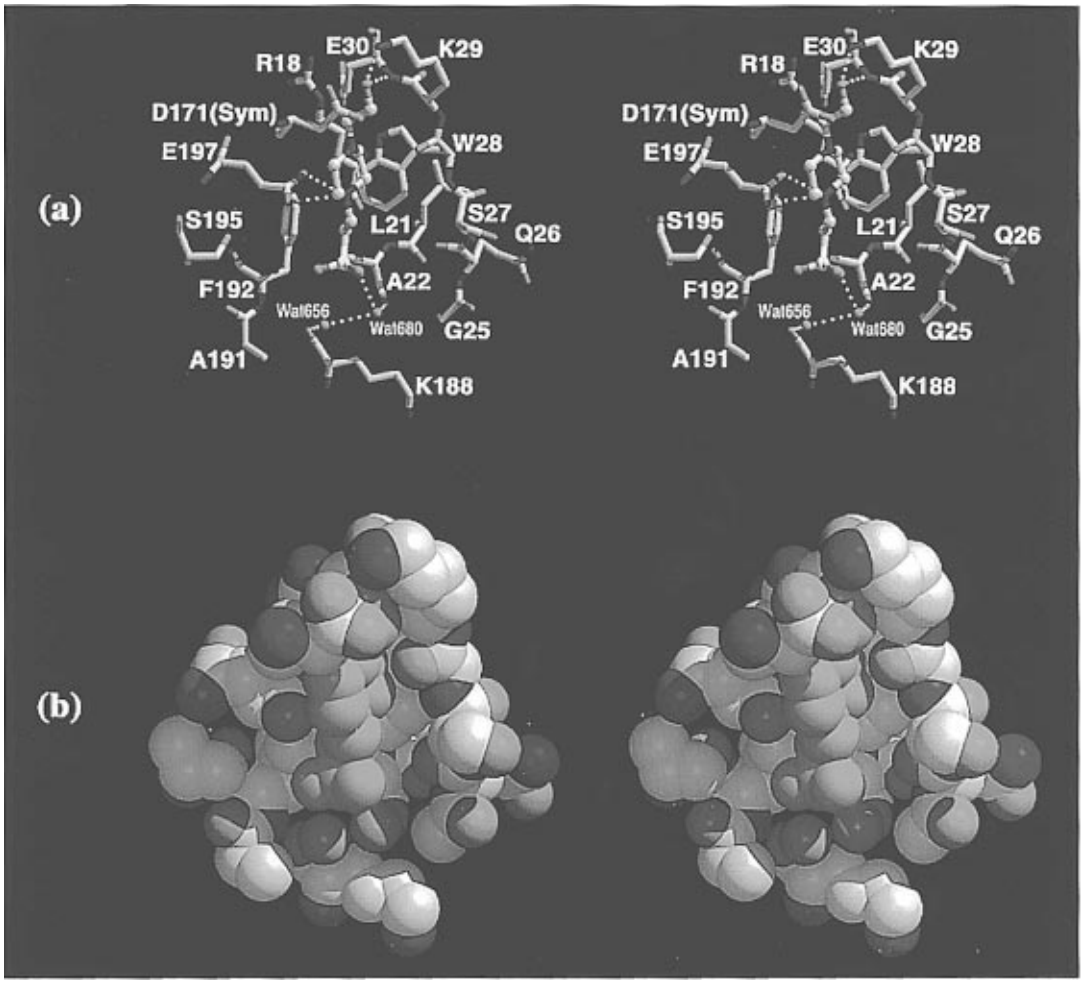

FIGURE 6: HEPES-binding site of hGSTP1-1[V104]. The site fits the description of a non-substrate-binding site of GSTs (*63*). It has a hydrophobic surface consisting of the aliphatic portion of the R18 side chain and hydrophobic side chains of A22, W28, and F192. Both the ball-and-stick model (a) and the space-filling model (b) are illustrated in the CPK color scheme with gray carbon, red oxygen, blue nitrogen, and yellow sulfur atoms. Hydrogen bonds are shown as dotted lines (a). Residues are labeled in panel a only. D171(Sym) represents the residue from a symmetry-related molecule (see the text). The representation was prepared by using TkRaster3D (see the legend to Figure 1 for details).

Table 4: Distances between the Hydroxyl Group of Y7 and the Sulfur Atom of Product Complexes Observed in Seven Crystal Structures of Class π GSTs

				O−S distance	
isozyme	PDB ID code[a]	resolution (Å)	product molecule	subunit A	subunit B
hGSTP1-1[V104]	1PGT	1.8	GSHex	3.2	3.2
hGSTP1-1[V104]	2PGT	1.9	GSPhen	3.2	3.2
hGSTP1-1[I104]	1GSS	2.8	GSHex	4.0	2.8
pGSTP1-1	2GSR	2.1	GSSAc	3.4	3.6
mGSTP1-1[b]	1GLP	1.9	GSSAc	3.6	3.5
mGSTP1-1	1GLQ	1.8	GSpNB	3.2	3.3
mGSTP1-1	2GLR	2.2	GSHex	3.5	3.2

[a] 1PGT and 2PGT (this work); 1GSS (*8*); 2GSR (*55*); and 1GLP, 1GLQ, and 2GLR (*51*). [b] The "Y"-based nomenclature (*65*) has been applied to the mouse GSTs (*66*−*68*).

residue I104 does assume different conformations in the two subunits of hGSTP1-1[I104] (*8*), the disturbance of the water structure by the introduction of the methyl group is the same. The interaction between water 1 and R13 and the continuation of the water network from the H-site to the surface of the enzyme may play important roles in the catalysis of class π GSTs. Therefore, the interruption of the hydrogen bond between water 1 and R13 and that between waters 4 and 4a would be expected to alter the catalytic ability of the enzyme.

We propose that the hydrophilic portion of the H-site is regulated by a hydrophobic residue at position 104. In an analogous situation, it has been shown that the amino acid difference at position 104 between mGSTP1-1 and mGSTP2-2 (valine or glycine, respectively) has been shown to be responsible for the different activities of these two enzymes (*56*). Finally, it has recently been demonstrated that hGSTP1-1[V104] is indeed a much better catalyst than hGSTP1-1[I104] in the GSH conjugation of diol epoxides of polycyclic aromatic hydrocarbons, including 7,8-dihydroxy-9,10-oxy-7,8,9,10-tetrahydrobenzo[*a*]pyrene (BPDE).[3]

The architecture of the H-site in class π GSTs appears to be complex, since a hydrophobic region lies next to a hydrophilic region, and the hydrophilic region is in turn regulated by a hydrophobic residue at position 104. This arrangement has obvious advantages if the xenobiotic substrate is hydrophobic but bears hydrophilic groups, e.g., the hydroxyl groups of BPDE. BPDE is believed to be the ultimate carcinogenic metabolite of benzo[*a*]pyrene (*57*−*59*). BPDE exists as a pair of diastereomers (*syn* and *anti*), and each diastereomer can be resolved into a pair of optical enantiomers (*58*). Of the four isomers, (+)-*anti*-BPDE (Scheme 1) has been shown to be the most potent carcinogen

[3] Personal communication.

in experimental animals *in vivo* (*58*, *60*). Isozyme hGSTP1-1 plays a major role in the detoxification of (+)-*anti*-BPDE in humans (*61*), presumably because the H-site in class π GSTs has both a hydrophobic and a hydrophilic region. The BPDE ring system might interact with the hydrophobic region of the H-site and the hydroxyl groups of BPDE with the hydrophilic region, which could stabilize the reaction intermediate. Since both the BPDE molecule and the H-site of hGSTP1-1 are polarized in terms of hydrophobicity and hydrophilicity, the enzyme is stereoselective toward BPDE. A three-dimensional structure of hGSTP1-1 complexed with the product of GSH addition to BPDE should shed light on the structural basis for the stereoselectivity of the enzyme.

The architecture of the class π H-site requires that a GST inhibitor able to selectively inhibit the class π isozymes should have a hydrophobic portion (e.g., the benzopyrene ring system of BPDE) and also bear hydrophilic groups (e.g., the hydroxyl groups of BPDE) to appropriately match the H-site. The H-site in all GSTs is relatively large. An isozyme specific inhibitor must be large enough to fill the site; a small xenobiotic moiety will be accommodated by the H-site of different classes of GSTs and will therefore have poor selectivity. Both the size and the hydrophobic/hydrophilic character of the inhibitor must be chosen to match the specific H-site in the target enzyme.

HEPES-Binding Site. One HEPES molecule is bound in the cavity between secondary structure elements β2 and αI (Figure 1). The bottom of the cavity is a hydrophobic surface formed by the side chains of R18, A22, W28, and F192, whereas a few potential hydrogen bond donor and acceptor groups are located on the edge of the cavity (Figure 6). Covering the hydrophobic bottom of the cavity, the HEPES molecule is stabilized by forming a few hydrogen bonds with the protein. There are three electrostatic interactions, seen in both subunits of the two structures, between the HEPES molecule and the protein, including the hydrogen bonds between the HEPES OH and E30 amide group, between the HEPES N1 and E197 side chain carboxyl group, and between the HEPES SO_3 and A22 carbonyl group via a bridging water molecule (Figure 6a). There is also a HEPES−protein interaction between HEPES N1 and K29 NZ, but it is not seen in every structure. Also shown in Figure 6 is the fact that the side chain of D171 from a symmetry-related molecule is in the vicinity of the OH end of the HEPES molecule, which suggests the possibility of a crystal-packing effect on HEPES binding. However, D171(symmetry) does not prevent the HEPES molecule from being exposed to the solvent (Figure 6b). Molecular modeling suggests that, with or without the HEPES molecule, the side chain of D171(symmetry) can form a salt bridge with the side chain of K29. It seems that the HEPES molecule is bound to the cavity before crystallization occurs. Moreover, the HEPES-binding mode in hGSTP1-1[V104] is different in many respects from those observed previously.

The HEPES molecule resembles an elongated sulfate anion (Figures 1 and 6), and it also behaves like a sulfate anion. HEPES interacts with residues that have positive charges such as arginine and lysine in two crystal structures: that of avian sarcoma virus integrase (*30*) and that of human dual-specific protein tyrosine phosphatase (*31*). In the structure of the integrase, the HEPES molecule is wedged completely between primary and symmetry-related molecules, whereas in the structure of the phosphatase, a HEPES molecule is bound in subunit A. In subunit B, however, the same binding site is occupied by a sulfate anion. These two examples are similar in that HEPES is bound between the primary molecule and a symmetry-related molecule, with the HEPES CH_2OH group interacting with a lysine residue from a symmetry-related molecule and the HEPES SO_3 group interacting extensively with the backbone amide groups, with the arginine side chain groups, and with the carbonyl group via water molecules. It is reasonable to conclude that the HEPES molecule is actually bound to a sulfate anion-binding site. Binding occurs when HEPES is available and the space is big enough for an "elongated" sulfate anion, and when binding favors both polar and nonpolar interactions with the protein.

The HEPES molecule found in the structure of hGSTP1-1[V104] has a binding mode different from that described above. First, the HEPES CH_2OH group forms a hydrogen bond to the amide group of E30, although it may also form a hydrogen bond to atom NZ of K29. Second, the HEPES SO_3 group does not interact with any positively charged sides chains, although it does form an indirect hydrogen bond to the carbonyl group of A22 via a water molecule. Third, the most important interaction between the HEPES molecule and the enzyme is the electrostatic interaction between the HEPES N1 and both OE1 and OE2 of E197 (Figure 6a). Fourth, the HEPES-binding site identified in hGSTP1-1 is not a sulfate-binding site. Located at the edges of this hydrophobic cavity, residues K29 and E197 are conserved in human, mouse, and pig GSTP1-1. This binding site may have some significance with respect to the function of the enzyme.

It has been reported recently that retinoids noncompetitively inhibit mammalian GSTs, especially isozymes from human placenta (*62*), suggesting the existence of a ligand-binding site distinct from the active site. The HEPES-binding site described in the present paper could also be the retinoic acid-binding site. Bico *et al*. (*63*) reported that both 8-anilino-1-naphthalene sulfonate and bromosulfophthalein bind to porcine class π GST (pGSTP1-1) at this site. The site has a highly hydrophobic surface, and occupation of the site inhibits catalytic function with GSH and CDNB in a noncompetitive manner. The HEPES-binding site found in the structure of hGSTP1-1[V104] has a hydrophobic surface consisting of the aliphatic portion of side chain R18 and hydrophobic side chains A22, W28, and F192 (Figure 6a). This site matches the description of the binding site proposed by Bico *et al*. (*63*), suggesting that the HEPES-binding site found in the crystal structures of hGSTP1-1[V104] is potentially this regulatory binding site.

Very recently, it has been suggested that in a class π GST from human skin residues 183−188 (LSARPK) are part of the H-site (*64*). hGSTP1-1 from placenta has the same conserved sequence. However, in our structure, the above fragment is about 25 Å away from the active site and is not directly part of the H-site. Residues 183−188 belong to the loop between αG and αH and the N end of αH (Figure 1). The next secondary structure element is αI followed by the C-terminal tail of the protein. The C-terminal tail forms part of the H-site in α, μ, π, σ, and Sj GSTs. As discussed in the previous sections, N204 and G205 in the C-terminal tail are H-site-defining residues in hGSTP1-1. The HEPES molecule in the hGSTP1-1[V104] structure interacts directly with E197 on αI (Figure 6). If a nonsubstrate molecule binds

at the HEPES-binding site, it may alter the physical and/or chemical property of the C-terminal tail and therefore influence xenobiotic substrate binding. Also, as shown in Figure 6, K188 is at the "bottom" of the HEPES-binding site and is involved in the binding of HEPES to hGSTP1-1 via two ordered water molecules (Figure 6a). We believe that residues 183−188 are involved in nonsubstrate binding of human GSTP1-1 and thus indirectly regulate the H-site, rather than being part of the H-site structure.

Conclusions. The crystal structures of the complexes of a class π GST with either GSHex or (9*R*,10*R*)-GSPhen reveal that the xenobiotic substrate-binding site in the class π enzyme is located at a position similar to that observed in the class μ isozyme. Unlike the hydrophobic cavity in the class μ GST, the xenobiotic substrate-binding site in the class π enzyme is approximately half hydrophobic and half hydrophilic. The hydrophilic portion of the cavity is in turn regulated by a hydrophobic residue at position 104. There is a short hydrogen bond (2.5 Å) between the Y108 (OH) and (9*R*,10*R*)-GSPhen (O5), indicating that the hydroxyl group of Y108 is an electrophilic participant in the addition of glutathione to epoxides. The binding site of a HEPES molecule fits a possible non-substrate-binding site that is involved in noncompetitive inhibition of the enzyme.

ACKNOWLEDGMENT

We thank Drs. Richard N. Armstrong, Stephen Hughes, and Alexander Wlodawer for their critical reading of the manuscript.

REFERENCES

1. Armstrong, R. N. (1991) *Chem. Res. Toxicol. 4*, 131−140.
2. Armstrong, R. N. (1994) *Adv. Enzymol. Relat. Areas Mol. Biol. 69*, 1−44.
3. Armstrong, R. N. (1997) *Chem. Res. Toxicol. 10*, 2−18.
4. Sinning, I., Kleywegt, G. J., Cowan, S. W., Reinemer, P., Dirr, H. W., Huber, R., Gilliland, G. L., Armstrong, R. N., Ji, X., Board, P. G., Olin, B., Mannervik, B., and Jones, T. A. (1993) *J. Mol. Biol. 232*, 192−212.
5. Ji, X., Zhang, P., Armstrong, R. N., and Gilliland, G. L. (1992) *Biochemistry 31*, 10169−10184.
6. Raghunathan, S., Chandross, R. J., Kretsinger, R. H., Allison, T. J., Penington, C. J., and Rule, G. S. (1994) *J. Mol. Biol. 238*, 815−832.
7. Reinemer, P., Dirr, H. W., Ladenstein, R., Schaffer, J., Gallay, O., and Huber, R. (1991) *EMBO J. 10*, 1997−2005.
8. Reinemer, P., Dirr, H. W., Ladenstein, R., Huber, R., Lo Bello, M., Federici, G., and Parker, M. W. (1992) *J. Mol. Biol. 227*, 214−226.
9. Ji, X., von Rosenvinge, E. C., Johnson, W. W., Tomarev, S. I., Piatigorsky, J., Armstrong, R. N., and Gilliland, G. L. (1995) *Biochemistry 34*, 5317−5328.
10. Wilce, M. C., Board, P. G., Feil, S. C., and Parker, M. W. (1995) *EMBO J. 14*, 2133−2143.
11. Reinemer, P., Prade, L., Hof, P., Neuefeind, T., Huber, R., Zettl, R., Palme, K., Schell, J., Koelln, I., Bartunik, H. D., and Bieseler, B. (1996) *J. Mol. Biol. 255*, 289−309.
12. Lim, K., Ho, J. X., Keeling, K., Gilliland, G. L., Ji, X., Ruker, F., and Carter, D. C. (1994) *Protein Sci. 3*, 2233−2244.
13. Hebert, H., Schmidt-Krey, I., and Morgenstern, R. (1995) *EMBO J. 14*, 3864−3869.
14. Ji, X., Armstrong, R. N., and Gilliland, G. L. (1993) *Biochemistry 32*, 12949−12954.
15. Ji, X., Johnson, W. W., Sesay, M. A., Dickert, L., Prasad, S. M., Ammon, H. L., Armstrong, R. N., and Gilliland, G. L. (1994) *Biochemistry 33*, 1043−1052.
16. Shan, S., and Armstrong, R. N. (1994) *J. Biol. Chem. 269*, 32373−32379.
17. Johnson, W. W., Liu, S., Ji, X., Gilliland, G. L., and Armstrong, R. N. (1993) *J. Biol. Chem. 268*, 11508−11511.
18. Oakley, A. J., Rossjohn, J., Lo Bello, M., Caccuri, A. M., Federici, G., and Parker, M. W. (1997) *Biochemistry 36*, 576−585.
19. Sato, K., Kitahara, A., Satoh, K., Ishikawa, T., Tatematsu, M., and Ito, N. (1984) *Jpn. J. Cancer Res. 75*, 199−202.
20. Sugioka, Y., Fujii-Kuriyama, Y., Kitagawa, T., and Muramatsu, M. (1985) *Cancer Res. 45*, 365−378.
21. Suguoka, Y., Kano, T., Okuda, A., Sakai, M., Kitagawa, T., and Muramatsu, M. (1985) *Nucleic Acids Res. 13*, 6049−6057.
22. Sato, K. (1988) *Jpn. J. Cancer Res. 79*, 556−572.
23. Sato, K. (1989) *Adv. Cancer Res. 52*, 205−255.
24. Muramatsu, M., Suzuki, T., Hisatake, K., and Okuda, A. (1995) in *Glutathione S-Transferease−Structure, Function and Clinical Implications* (Vermeulen, N. P. E., Mulder, G. J., Nieuwenhuyse, H., Peters, W. H. M., and van Bladeren, P. J., Eds.) pp 85−95, Taylor & Francis, London.
25. Morgan, A. S., Ciaccio, P. J., Tew, K. D., and Kauvar, L. M. (1996) *Cancer Chemother. Pharmacol. 37*, 363−370.
26. Board, P. G., Webb, G. C., and Coggan, M. (1989) *Ann. Hum. Genet. 53*, 205−213.
27. Ahmad, H., Wilson, D. E., Fritz, R. R., Singh, S. V., Medh, R. D., Nagle, G. T., Awasthi, Y. C., and Kurosky, A. (1990) *Arch. Biochem. Biophys. 278*, 398−408.
28. Zimniak, P., Nanduri, B., Pikula, S., Bandorowicz-Pikula, J., Singhal, S. S., Srivastava, S. K., Awasthi, S., and Awasthi, Y. C. (1994) *Eur. J. Biochem. 224*, 893−899.
29. Mannervik, B., Bjornestedt, R., Davey, E., Emahazion, T., Fernandez, E., Hansson, L. O., Kolm, R. H., Nilsson, L. O., Olin, B., Stenberg, G., Tardioli, S., Widersten, M., and Yilmaz, S. (1995) in *Glutathione S-Transfereases−Structure, Function and Clinical Implications* (Vermeulen, N. P. E., Mulder, G. J., Nieuwenhuyse, H., Peters, W. H. M., and van Bladeren, P. J., Eds.) pp 3−11, Taylor & Francis, London.
30. Bujacz, G., Jaskolski, M., Alexandratos, J., Wlodawer, A., Merkel, G., Katz, R. A., and Skalka, A. M. (1995) *J. Mol. Biol. 253*, 333−346.
31. Yuvaniyama, J., Denu, J. M., Dixon, J. E., and Saper, M. A. (1996) *Science 272*, 1328−1331.
32. McTigue, M. A., Williams, D. R., and Tainer, J. A. (1995) *J. Mol. Biol. 246*, 21−27.
33. Ji, X., von Rosenvinge, E. C., Johnson, W. W., Armstrong, R. N., and Gilliland, G. L. (1996) *Proc. Natl. Acad. Sci. U.S.A. 93*, 8208−8213.
34. Simons, P. C., and Vander Jagt, D. L. (1977) *Anal. Biochem. 82*, 334−341.
35. Chung, H. S., Harvey, R. G., Armstrong, R. N., and Jarabak, J. (1987) *J. Biol. Chem. 262*, 12448−12451.
36. Otwinowski, Z., and Minor, W. (1997) *Methods Enzymol. 276A*, 307−326.
37. Rossman, M. G. (1972) *Molecular Replacement Method*, Gordon and Breach, New York.
38. Navaza, J. (1994) *Acta Crystallogr. A 50*, 157−163.
39. Collaborative Computational Project, Number 4 (1994) *Acta Crystallogr. D 50*, 760−763.
40. Brunger, A. T. (1992) in *X-PLOR (Version 3.1) Manual*, pp 187−218, Yale University Press, New Haven, CT.
41. Furey, W., Wang, B., and Sax, M. (1982) *J. Appl. Crystallogr. 15*, 160−166.
42. Hendrickson, W., and Konnert, J. (1980) in *Computing in Crystallography* (Diamond, R., Ramaseshan, S., and Venkatesan, K., Eds.) pp 1301−1323, Indian Academy of Sciences, Bangalore, India.
43. Hendrickson, W., and Konnert, J. (1980) in *Biomolecular Structure, Function, Conformation and Evolution*, pp 43−57, Pergamon, Oxford.
44. Hendrickson, W. A. (1985) *Methods Enzymol. 115*, 252−270.
45. Hendrickson, W. A. (1985) in *Crystallographic Computing 3: Data Collection, Structure Determination, Proteins and Databases* (Sheldrick, G., Kruger, C., and Goddard, R., Eds.) pp 306−311, Clarendon Press, Oxford.
46. Jones, T. A., Zou, J. Y., Cowan, S. W., and Kjeldgaard, M. (1991) *Acta Crystallogr. A 47*, 110−119.
47. Bhat, T. N. (1988) *J. Appl. Crystallogr. 21*, 279−281.

48. James, M. N., and Sielecki, A. R. (1983) *J. Mol. Biol. 163*, 299−361.
49. Bernstein, F. C., Koetzle, T. F., Williams, G. J., Meyer, E. E., Jr., Brice, M. D., Rodgers, J. R., Kennard, O., Shimanouchi, T., and Tasumi, M. (1977) *J. Mol. Biol. 112*, 535−542.
50. Laskowski, R. A. (1993) *J. Appl. Crystallogr. 26*, 283−291.
51. Garcia-Saez, I., Parraga, A., Phillips, M. F., Mantle, T. J., and Coll, M. (1994) *J. Mol. Biol. 237*, 298−314.
52. Liu, S., Zhang, P., Ji, X., Johnson, W. W., Gilliland, G. L., and Armstrong, R. N. (1992) *J. Biol. Chem. 267*, 4296−4299.
53. Liu, S., Ji, X., Gilliland, G. L., Stevens, W. J., and Armstrong, R. N. (1993) *J. Am. Chem. Soc. 115*, 7910−7911.
54. Zheng, Y.-A., and Ornstein, R. L. (1997) *J. Am. Chem. Soc. 119*, 1523−1528.
55. Dirr, H., Reinemer, P., and Huber, R. (1994) *J. Mol. Biol. 243*, 72−92.
56. Bammler, T. K., Driessen, H., Finnstrom, N., and Wolf, C. R. (1995) *Biochemistry 34*, 9000−9008.
57. Weinstein, I. B., Jeffrey, A. H., Leffler, S., Pulkrabek, P., Yamasaki, H., and Grunberger, D. (1978) in *Polycyclic Hydrocarbons and Cancer* (Gelboin, H. V., and Ts'o, P. O. P., Eds.) pp 4−36, Academic Press, New York.
58. Buening, M. K., Wislocki, P. G., Levin, W., Yagi, H., Thakker, D. R., Akagi, H., Koreeda, M., Jerina, D. M., and Conney, A. H. (1978) *Proc. Natl. Acad. Sci. U.S.A. 75*, 5358−5361.
59. Gelboin, H. V. (1980) *Physiol. Rev. 60*, 1107−1166.
60. Slaga, T. J., Bracken, W. J., Gleason, G., Levin, W., Yagi, H., Jerina, D. M., and Conney, A. H. (1979) *Cancer Res. 39*, 67−71.
61. Robertson, I. G., Guthenberg, C., Mannervik, B., and Jernstrom, B. (1986) *Cancer Res. 46*, 2220−2224.
62. Kulkarni, A. A., and Kulkarni, A. P. (1995) *Cancer Lett. 91*, 185−189.
63. Bico, P., Erhardt, J., Kaplan, W., and Dirr, H. (1995) *Biochim. Biophys. Acta 1247*, 225−230.
64. Whalen, R., Kempner, E. S., and Boyer, T. D. (1996) *Biochem. Pharmacol. 52*, 281−288.
65. Bass, N. M., Kirsch, R. E., Tuff, S. A., Marks, I., and Saunders, S. J. (1977) *Biochim. Biophys. Acta 492*, 163−175.
66. Hayes, J. D., Coulthwaite, R. E., Stockman, P. K., Hussey, A. J., Mantle, T. J., and Wolf, C. R. (1987) *Arch. Toxicol. Suppl. 10*, 136−146.
67. McLellan, L. I., and Hayes, J. D. (1989) *Biochem. J. 263*, 393−402.
68. Hayes, J. D., and Pulford, D. J. (1995) *Crit. Rev. Biochem. Mol. Biol. 30*, 445−600.
69. Bacon, D. J., and Anderson, W. F. (1988) *J. Mol. Graphics 6*, 219−220.
70. Kraulis, P. J. (1991) *J. Appl. Crystallogr. 24*, 946−950.

BI970805S